Physics of the Solid State, 2024, Vol. 66, No. 11

06,08

Polar properties of spherulite thin films of lead zirconate-titanate obtained by high-temperature annealing from an amorphous phase

© A.R. Valeeva[1], I.P. Pronin[1], E.Yu. Kaptelov[1], S.V. Senkevich[1], M.V. Staritsyn[1,2], D.A. Kiselev[3], S.A. Nemov[4]

[1] Ioffe Institute,
St. Petersburg, Russia
[2] National Research Center „Kurchatov Institute“ — Central Research Institute
of Structural Materials „Prometey“ named after I.V. Gorynin,
St. Petersburg, Russia
[3] National University of Science and Technology „MISiS“,
Moscow, Russia
[4] Peter the Great Saint-Petersburg Polytechnic University,
St. Petersburg, Russia
E-mail: Petrrovich@mail.ioffe.ru

Received November 12, 2024
Revised November 13, 2024
Accepted November 14, 2024

The effect of the microstructure (block size and new intrablock boundaries) of spherulite thin films of lead zirconate titanate on the magnitude of the internal field and self-polarization is studied. The films, whose composition corresponded to the region of the morphotropic phase boundary, were formed by a two-stage method of high-frequency magnetron sputtering. It is shown that the magnitude of the radial-lateral tensile mechanical stresses changes as the size of the blocks increases, leading to a redistribution of the negative space charge (electrons) in the volume of the thin film. A possible contribution to the formation of self-polarization of the space charge of oxygen vacancies caused by their directed diffusion is considered.

Keywords: thin films of lead zirconate-titanate, spherulite microstructure, lateral mechanical stresses, internal field, self-polarization, directed diffusion of oxygen vacancies.

DOI: 10.61011/PSS.2024.11.60098.304

1. Introduction

Recently, researchers have been increasingly interested in crystal structures, which are synthesized during high-temperature annealing of thin amorphous films previously deposited on a cold substrate. This is attributable to the increasing use of thin-film materials in a variety of applications in order to miniaturize, save energy, and speed up devices and devices. In the absolute majority, crystallization of amorphous films occurs through the nucleation of islands, their subsequent proliferation and fusion with formation of a polycrystalline structure.

Crystallization from the amorphous phase is accompanied by a change (usually an increase) of the density of the films which results in the formation of a flat cylinder shape of a growing island under the impact of radial mechanical stresses. Such a spherulite-type formation is widespread in case of the crystallization of thin films, regardless of their composition and the symmetry of the crystal lattice [1–5]. The features of such spherulite films are the formation of a radially radiant microstructure by small-angle non-crystalline branching, accompanied by a radial reversal of the crystal lattice [1–9]. As a rule, the angle of rotation linearly increases with the increase of the radius of spherulite island. Such structures are often attributed to the type of so-called rotational crystals [2,8].

Spherulite microstructure is often observed in thin ferroelectric films, including lead zirconate-titanate $Pb(Zr,Ti)O_3$(PZT) films formed by both physical and chemical methods [5,8–13]. The interest in these compounds is primarily attributable to their increasing use in microelectromechanics [14–16]. It is important for the effective use in microelectromechanics devices that the formed films have a macroscopic polarization — unipolarity (or self-polarization) comparable in magnitude to spontaneous (or residual) polarization. It should be noted that the presence of self-polarization leads to greater stability of the polar state [17–19]. The formation of a macroscopic polar state in a thin ferroelectric film during its preparation is usually associated with the polarizing effect of a space charge formed near the interface between the thin film and the lower electrode previously deposited on the substrate. Typically, the space charge at the lower interface is formed in PZT thin films as a result of electron condensation on deep traps. It is important that the positive charge in the form of positively charged oxygen vacancies is localized in the upper part of the film, which would contribute to the formation of macroscopic polarization throughout the entire volume of the film.

The bending deformation of the crystal lattice, leading to the formation of an internal field is another possible mechanism for the formation of self-polarization. Until recently, the popular version remains that the formation of self-polarization is attributable to the flexoelectric effect associated with the mutual displacement of atoms of different types within the unit cell under bending action on a thin film because of differences in the values of the temperature coefficient of linear expansion of the thin film and the substrate [20,21]. However, calculations indicate that its effect is too weak in real conditions [22]. This determines the need to search for other mechanisms that contribute to the reorientation of ferroelectric dipoles in the direction of the mechanical stress gradient.

The effect of directed (upward) diffusion of oxygen vacancies, which is commonly referred to as the Gorsky effect, can be attributed to such mechanisms [23–25]. Since there is a rather strong reversal of the crystal lattice in PZT spherulite films and, consequently, deformation of the crystal lattice, it could be expected that the effect has a significant impact on the diffusion of oxygen vacancies in PZT films.

The aim of this study was to compare the formation of an internal field and self-polarization due to the formation of a negative space charge at the lower interface of the film, and due to the directed diffusion of oxygen vacancies in PZT spherulite thin films in which the deformation of the crystal lattice depended on the average size of the spherulite blocks [5].

2. Objects and methods of research

Thin PZT films of $PbZr_{0.54}Ti_{0.46}O_3$ composition obtained by the two-stage RF magnetron sputtering method were selected to study the effect. Amorphous films were deposited on substrates at a low temperature at the first stage, and at the second stage, to crystallize the perovskite phase, they were subjected to high-temperature annealing at 580°C for 1 hour, followed by slow cooling in the oven. The size of the spherulite blocks was increased by reducing the distance from the target to the substrate (D) in the range of 70−30 mm. The block size reached the maximum values of $\sim 40{-}50\,\mu$m at $D = 30$ mm [5]. The film thickness was 500 nm. A platinized silicon wafer was the substrate. The composition of the sprayed ceramic PZT target corresponded to the region of the morphotropic phase boundary, where the dielectric and electromechanical parameters reached maximum values [26].

Electronic images of thin films were obtained using a Lyra 3 scanning electron microscope (Tescan). The energy of the probing electron beam was 12 keV. The piezoelectric response force microscopy method MFP-3D SA (Asylum Research) was used to study the piezoelectric response. The measurements were conducted by applying 5 V alternating voltage to the cantilever at a frequency of 50 kHz. The area of the scanned surface was $40 \times 40\,\mu$m. Contact pads with a size of $\sim 100 \times 100\,\mu$m were applied to the free surface of the films for electrophysical measurements. An automated system based on E7-20 immittance meter was used to study dielectric properties. Dielectric hysteresis loops were studied using a modified Sawyer-Tower circuit.

3. Experimental results and discussion thereof

Figure 1 shows diffraction maps of reflected electrons obtained on films deposited at $D = 60$, 40 and 30 mm ($a{-}c$, respectively). The maps indicate an increase of the size of the spherulite blocks with a decrease of the target-substrate distance. An increase of the block size, in turn, leads to an increase of the rate of rotation of the crystal lattice — from 0.4−0.5 deg/μm at $D = 70$ mm to $\sim 1.4{-}1.5$ deg/μm for $D = 40$ mm. The deformation of the crystal lattice increases in proportion to the reversal rate according to the data provided in Ref. [2,3], reaching a value of $\sim 1.5\%$ [5]. In turn, the maximum mechanical stresses are estimated by the value ~ 580 MPa, close to the value of the elastic limit in PZT films [27]. Apparently, in reality, the magnitude of these stresses is somewhat lower, however, rather complex and expensive studies are required for a more accurate quantitative determination.

The reversal rate decreased (table) in films with maximum block sizes (deposited at $D = 30$ mm). We associate this with the appearance of additional large-angle open boundaries (Figure 1), most likely caused by the achievement of extreme elastic mechanical stresses. These boundaries represent areas of disruption of the crystal lattice with an increased concentration of dislocations and pores, which leads to partial relaxation of lateral mechanical stresses. A multiple increase of the lateral component of ferroelectric polarization (table) [5,9] also indicates an increase of tensile mechanical stresses with increasing block sizes, which contributes to the reorientation of polarization in directions as close as possible to the plane of the film (substrate).

Figure 2 shows images of the normal component of the piezoelectric response, the color palette of which reflects a change of the self-polarization value (P_{self}) of the films, and histograms of the distribution P_{self} over the scanning area of the studied samples. The magnitude of the shift of the histogram along the abscissa axis relative to the origin is proportional to the value P_{self}. Figure 3 shows the change of the value of P_{self} with an increase of D. It can be seen that the dependence $P_{\text{self}}(D)$ passes through a minimum at $D = 40$ mm, which corresponds to the maximum value of lateral polarization and the maximum values of tensile mechanical stresses.

The results of the study of the dielectric properties of films are shown in Figures 4 and 5. Figure 4 reflects

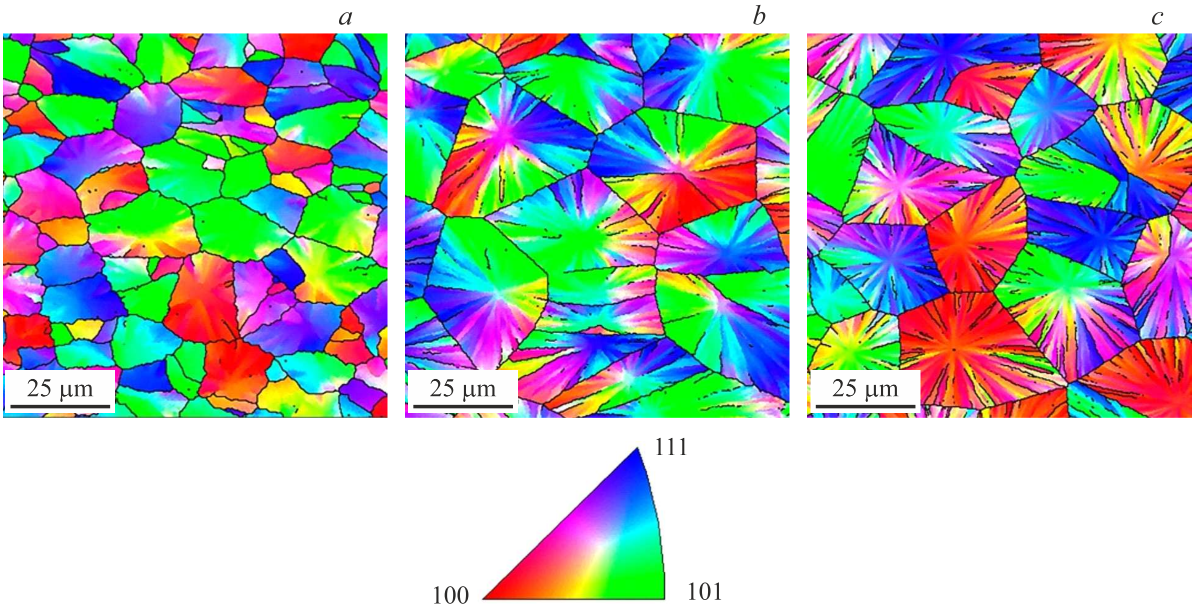

Figure 1. Maps of distribution of crystallographic axes normally oriented to the film plane for thin films deposited at a target-substrate distance of 60 (a), 40 (b) and 30 mm (c).

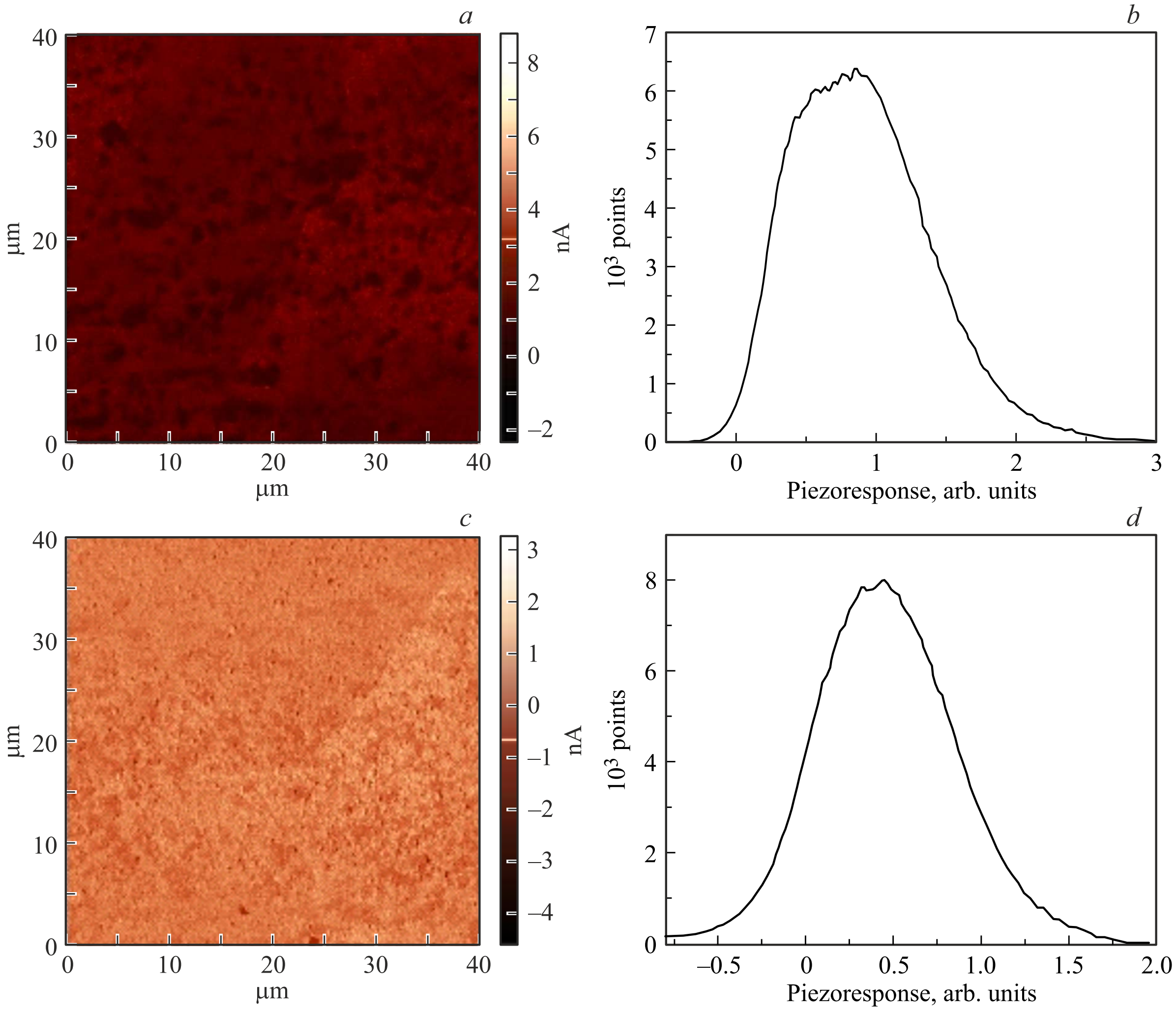

Figure 2. Map of the normal component of the piezoelectric response (a, c) and its distribution over the scanning area (b, d) of thin PZT films deposited at a target-substrate distance of 40 (a, b) and 60 mm (c, d).

Variation of the size of spherulite blocks, the rate of rotation of the crystal lattice, and lateral polarization in PZT films depending on the target-substrate distance

Target-substrate distance, mm	Average area of spherulite blocks, μm^2	Lattice rotation rate, deg/μm	Lateral component of polarization, arb. units
30	770	0.80	16
40	590	1.40	23
50	430	1.05	22
60	215	0.50	6.1
70	220	0.50	5.3

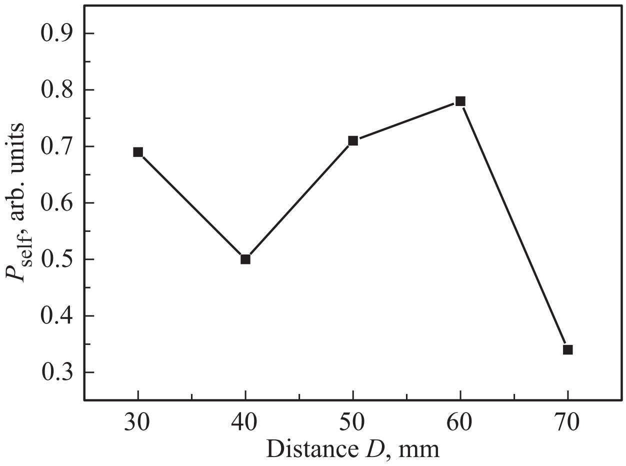

Figure 3. Self-polarization (P_{self}) of thin PZT films deposited at different target-substrate distances.

the shape of dielectric hysteresis loops (P−V) measured in an electric field with an amplitude of 200 kV/cm at a frequency of 1 kHz. Based on them, the dependence of the magnitude of the internal field (E_{int}), determined by the displacement of the loop along the axis of the abscissa, on the target-substrate distance is constructed (Figure 5). It can be seen from Figure 5 that E_{int} decreases sharply in the film deposited at $D = 40$ mm: this value $E_{int} = 10$ kV/cm is almost two times less than at neighboring points on the graph. At the same time, the maximum value of $E_{int} \sim 30$ kV/cm was observed in films characterized by a high concentration of open large-angle boundaries (at $D = 30$ mm). The magnitude of the internal field in PZT thin films according to the data of provided in Ref. [18,19] is determined by the magnitude of the negative space charge (electrons) localized at the lower interface of the ferroelectric film in the absence of the upper electrode, and the charge itself is determined by the concentration of charged oxygen vacancies. The magnitude of the self-polarization P_{self} is the result of the reorientation of ferroelectric dipoles under the action of a space charge field and depends on the distribution of the field over the thickness of the film, and, therefore, on the distribution of charged oxygen vacancies.

Ref. [5,9] show that an increase of tensile lateral (biaxial) mechanical stresses leads to a sharp increase of the signal of the second optical harmonic and, consequently, the lateral projection of polarization with maximum values in films deposited at $D = 40$mm (see table). Another consequence is the appearance of lateral-radial self-polarization, the vector of which is directed from the center of the spherulite island (or block) to the periphery. The direction of its vector is determined by the negative charge created by electrons localized in deep traps of the boundary of the perovskite island, and the radial orientation of ferroelectric dipoles with oxygen vacancies tied to them, evenly distributed in the volume of the film (Figure 6, *a*). The appearance of a space charge on the periphery of the islands (or blocks) means a redistribution of the negative charge, which leads to a decrease in the space charge at the lower interface of the film, and, as a result, to a decrease in the magnitude of the internal field E_{int} (Figure 5) and normally oriented polarization (P_{self}) (Figure 3). The formation of numerous large-angle boundaries in films deposited at $D = 30$ mm, means not only partial relaxation (i.e. reduction) of lateral mechanical stresses, but also the formation of conductive channels facilitating additional charging of the lower interface, and leading to an increase of both E_{int} and P_{self} (Figure 6, *b*).

When the crystal lattice is rotated with a gradient of mechanical stresses directed towards the substrate, Figure 6, a decrease of radial-lateral mechanical stresses should result in a redistribution of oxygen vacancies to the upper part of the film. We use the following formula to estimate the flux of oxygen vacancies (I_v) under the action of an elastic stress gradient, [28]:

$$I_v = N_v(D_v/kT)(\partial\sigma/\partial x)\omega_v, \quad (1)$$

where N_v — oxygen vacancy concentration, D_v — oxygen vacancy diffusion coefficient, k — Boltzmann constant, T — temperature, σ — mechanical stresses, ω_v — volume occupied by oxygen vacancy. According to the data provided in Ref. [29], the diffusion coefficient in PZT thin films at room temperature is characterized by the value $D_v \sim 5 \cdot 10^{-20}\,m^2$; $N_v \sim 10^{26}\,m^{-3}$ [30], $\sigma \sim 5 \cdot 10^{10}$ Pa, $\omega_v \sim 8 \cdot 10^{-30}\,m^3$. Hence, the flux of oxygen vacancies arising under the action of elastic stresses in a

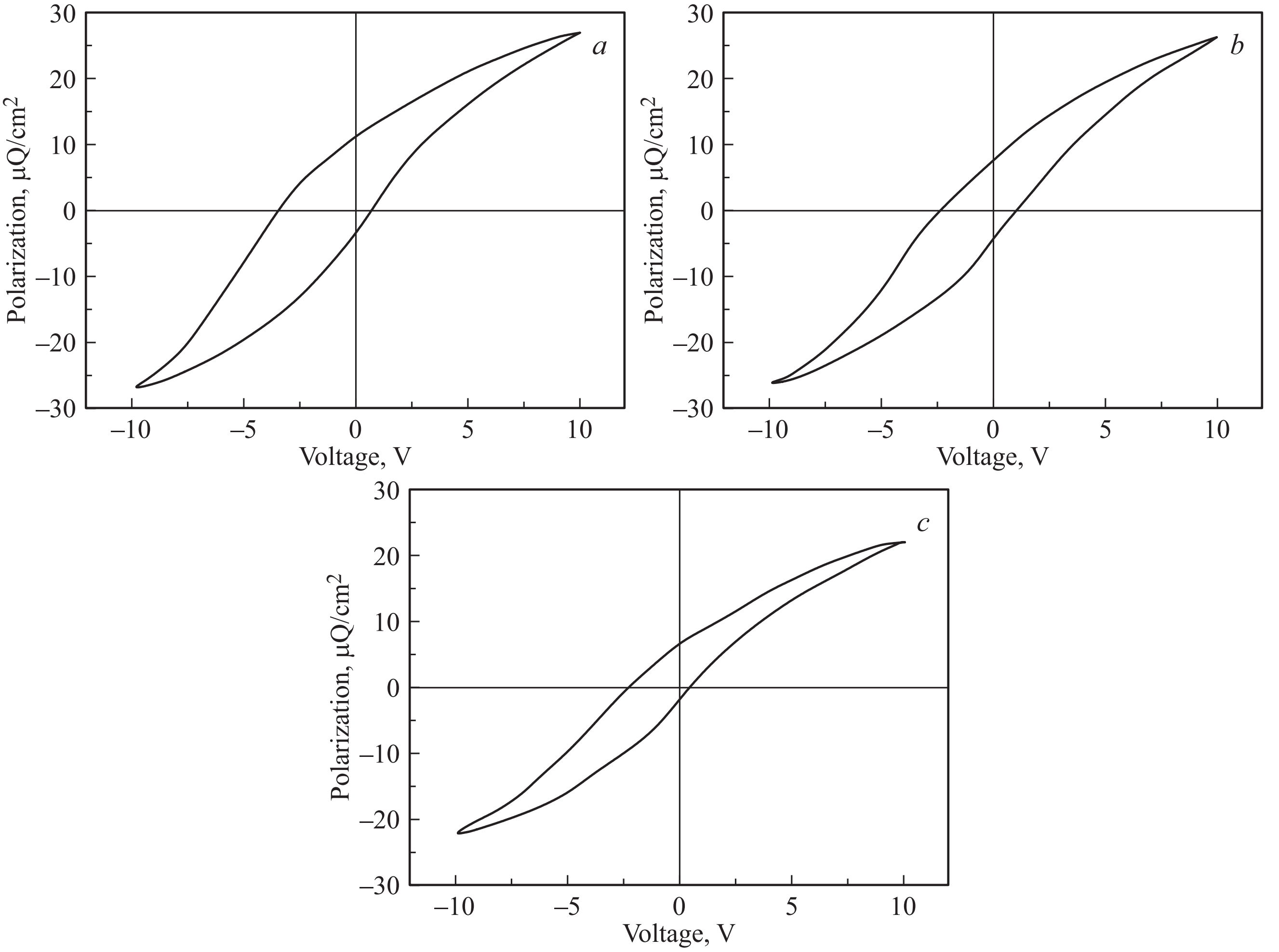

Figure 4. Dielectric hysteresis loops of thin PZT films deposited at a target-substrate distance of 30 (*a*), 40 (it b) and 70 mm (*c*). Frequency — 1 kHz.

500 nm thick film at room temperature is estimated as $I_v \sim 10^{13}\,\mathrm{m^{-2}\cdot s^{-1}}$.

However, at least two factors should be taken into account for a more accurate assessment of the diffusion rate. One of them is related to the fact that the spherulite structure is characterized by a high concentration of dislocations ($\sim 10^{17}\,\mathrm{m^{-2}}$ according to our estimate), because of which the flux of oxygen vacancies can increase by $\sim$ 4–5 orders of magnitude. Another factor is related to an exponential increase of the diffusion coefficient with temperature, which can lead to its increase by 3–4 orders of magnitude at the annealing temperature [30]. For this reason the estimated value of the vacancy rate can increase by 7–9 orders of magnitude taking into account these factors and amount to $\sim 10^{20}{-}10^{22}\,\mathrm{m^{-2}\cdot s^{-1}}$. This means that a large (or significant) part of the charged oxygen vacancies can move to the upper part of the thin film during the crystallization of the perovskite phase (over time $\sim 10^4$ s) (Figure 6, *b*). The formation of an internal field due to the volumetric charge of oxygen vacancies may be an alternative mechanism for the formation of self-polarization in this

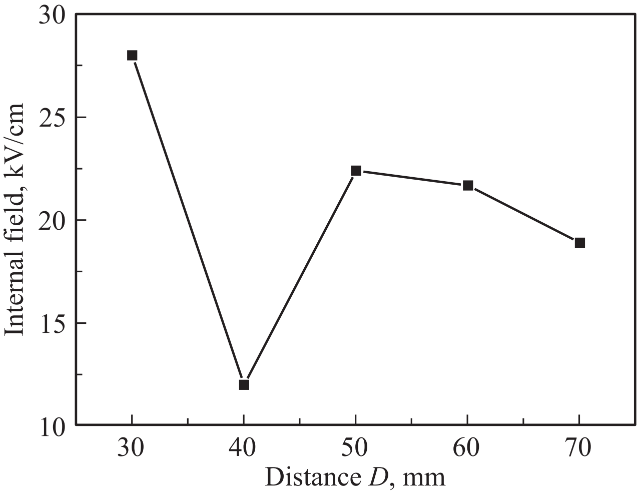

Figure 5. The change of the magnitude of the internal field (E_{int}), determined by dielectric hysteresis loops, for thin PZT films deposited at different target-substrate distances.

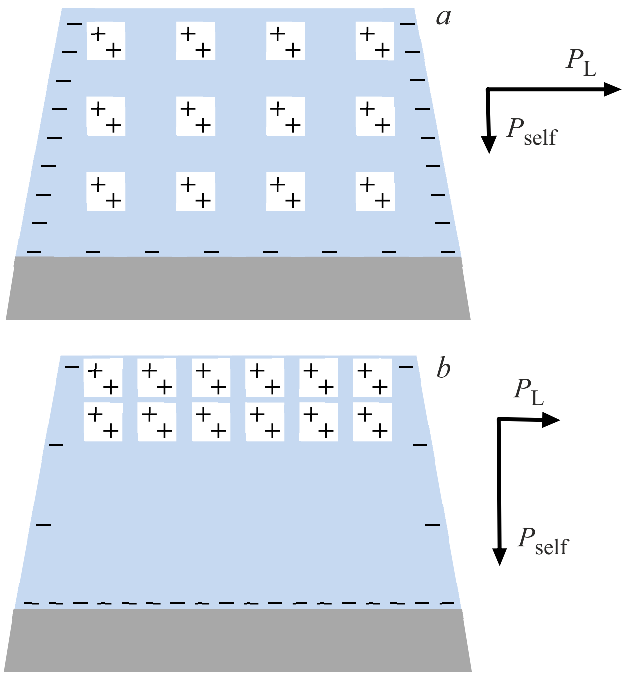

Figure 6. Diagram of the space charge distribution and the direction of the vectors of normally oriented self-polarization and lateral self-polarization.

case. However, additional studies are required to verify this version.

4. Conclusions

Experiments have shown that an increase of the size of spherulite blocks and the occurrence of new intrablock boundaries in thin ferroelectric PZT films leads to a change of lateral mechanical stresses and, as a result, to a change of the conditions of the formation of a space charge and a significant change of the internal field and self-polarization values. The explanation of the observed effects is based on established ideas about the nature of the formation of an internal field and self-polarization associated with the formation of a negative space charge. Nevertheless, the effects observed in PZT thin films caused by the deformation of the crystal lattice under the action of lateral mechanical stresses indicate that it is necessary to take into account the contribution of directed diffusion of oxygen vacancies to the formation of self-polarization at the perovskite phase crystallization stage.

Funding

This study was supported by grant No. 24-22-00631 from the Russian Science Foundation.

Conflict of interest

The authors declare that they have no conflict of interest.

References

[1] A.G. Shtukenberg, Yu.O. Punin, E. Gunn, B. Kahr. Chem. Rev. **112**, *3*, 1805 (2012).
[2] V.Yu. Kolosov, A.R. Thölén. Acta Mater. **48**, 1829 (2000).
[3] E.J. Musterman, V. Dierolf, H. Jain. Int. J. Appl. Glass Sci. **13**, *3*, 402 (2022).
[4] B. Da, L. Cheng, X. Liu, K. Shigeto, K. Tsukagoshi, T. Nabatame, Z. Ding, Y. Sun, J. Hu, J. Liu, D. Tang, H. Zhang, Z. Gao, H. Guo, H. Yoshikawa, S. Tanuma. Sci. Technol. Adv. Mater. Meth. **3**, *1*, 2230870 (2023).
[5] M.V. Staritsyn, V.P. Pronin, I.I. Khinich, S.V. Senkevich, E.Yu. Kaptelov, I.P. Pronin, A.S. Elshin, E.D. Mishina. Phys. Solid State **65**, *8*, 1312 (2023).
[6] N.R. Lutjes, S. Zhou, J. Antoja-Lleonart, B. Noheda, V. Ocelík. Sci. Rep. **11**, 14888 (2021).
[7] B.J. Kooi, J.Th.M. De Hosson. J. Appl. Phys. **95**, 4714 (2004).
[8] O.M. Zhigalina, D.N. Khmelenin, Y.A. Valieva, V.Yu. Kolosov, K.A. Kuznetsov, A.O. Bokunyaeva, K.A. Vorotilov, A.S. Sigov. Crystallography Reports **63**, *4*, 646 (2018).
[9] A.S. Elshin, I.P. Pronin, S.V. Senkevich, E.D. Mishina. Tech. Phys. Lett. **46**, *4*, 385 (2020).
[10] G.A.C.M. Spierings, V.J.B.A. an Zon, P.K. Larsen, M. Klee. Integr. Ferroelectr. **3**, *3*, 283 (1993).
[11] S.-Y. Chen, I.-W. Chen. J. Am. Ceram. Soc. **81**, *1*, 97 (1998).
[12] E.M. Alkoy, S. Alkoy, T. Shiosaki. Ceram. Int. **33**, *8*, 1455 (2007).
[13] I. Bretos, E. Rodrigez-Castellon, M. Tomczyk, R. Jimenez, P.M. Vilarinho, M.L. Calzada. Sci. Rep. **6**, 20143 (2016).
[14] P. Muralt, R.G. Polcawich, S. Trolier-McKinstry. MRS Bulletin **34**, *9*, 658 (2009).
[15] Y. Ma, J. Song, X. Wang, Y. Liu, J. Zhou. Coatings **11**, *8*, 944 (2021).
[16] L. Song, S. Glinsek, E. Defay. Appl. Phys. Rev. **8**, 041315 (2021).
[17] A.L. Kholkin, K.G. Brooks, D.V. Taylor, S. Hiboux, N. Setter. Integr. Ferroelectr. **22**, 525 (1998).
[18] V.P. Afanasjev, A.A. Petrov, I.P. Pronin, E.A. Tarakanov, A.V. Pankrashkin, E.Yu. Kaptelov, J. Graul. J. Phys. Condens. Matter **13**, 8755 (2001).
[19] N. Balke, I. Bdikin, S.V. Kalinin, A.L. Kholkin. J. Am. Ceram. Soc. **92**, *8*, 1629 (2009).
[20] E. Sviridov, I. Sem, V. Alyoshin, S. Biryukov, V. Dudkevich. MRS Online Proc. Lib. **361**, 141 (1994).
[21] L.A. Delimova, N.V. Zaitseva, V.V. Ratnikov, V.S. Yuferev, D.S. Seregin, K.A. Vorotilov, A.S. Sigov. Phys. Solid State **63**, *8*, 1145 (2021).
[22] A. Gruverman, B.J. Rodriguez, A.I. Kingon, R.J. Nemanich, A.K. Tagantsev, J.S. Cross, M. Tsukada. Appl. Phys. Lett. **83**, 728 (2003).
[23] W.S. Gorsky. Phys. Z. Sowjetunion **8**, 457 (1935).
[24] A.M. Kosevich. Usp. Fiziol. Nauk **114**, *3*, 509 (1974). (in Russian).

[25] I.P. Pronin, S.A. Kukushkin, V.V. Spirin, S.V. Senkevich, E.Yu. Kaptelov, D.M. Dolgintsev, V.P. Pronin, D.A. Kiselev, O.N. Sergeeva. Mater. Phys. Mech. **30**, *1*, 20 (2017).
[26] B. Yaffe, W. Cook, G. Yafe. Piezoelektricheskaya keramika. Mir, M. (1974). 288 s. (in Russian).
[27] D.E. Cox, B. Noheda, G. Shirane. Phys. Rev. B **71**, 134110 (2005).
[28] S.A. Kukushkin, A.V. Osipov. Pis'ma v ZhTF **43**, *13*, 81 (2017). (in Russian).
[29] G. Holzlechner, D. Kastner, C. Slouka, H. Hutter, J. Fleig. Solid State Ion. **262**, 625 (2014).
[30] B. Akkopru-Akgun, D.M. Marincel, K. Tsuji, T.J.M. Bayer, C.A. Randall, M.T. Lanagan, S. Trolier-McKinstry. J. Am. Ceram. Soc. **104**, *10*, 5270 (2021).

Translated by A.Akhtyamov